Sheffield Hallam University

Dry sliding wear mechanisms of HIPIMS plasma nitrided CoCrMo alloy for medical implant applications

ARUNACHALAM SUGUMARAN, Arunprabhu <http://orcid.org/0000-0002-5087-4297>, SHUKLA, Krishanand, KHAN, Imran, EHIASARIAN, Arutiun <http://orcid.org/0000-0001-6080-3946> and HOVESPIAN, Papken

Available from Sheffield Hallam University Research Archive (SHURA) at:

https://shura.shu.ac.uk/27739/

This document is the Accepted Version [AM]

Citation:

ARUNACHALAM SUGUMARAN, Arunprabhu, SHUKLA, Krishanand, KHAN, Imran, EHIASARIAN, Arutiun and HOVESPIAN, Papken (2020). Dry sliding wear mechanisms of HIPIMS plasma nitrided CoCrMo alloy for medical implant applications. Vacuum. [Article]

Copyright and re-use policy

See http://shura.shu.ac.uk/information.html

Sheffield Hallam University Research Archive
http://shura.shu.ac.uk

Dry sliding wear mechanisms of HIPIMS plasma nitrided CoCrMo alloy for medical implant applications

Arunprabhu Arunachalam Sugumaran[a]*, Krishnanand Shukla[a], Imran Khan[b], Arutiun Papken Ehiasarian[a], Papken Ehiasar Hovsepian[a]

a National HIPIMS Technology Centre, Materials and Engineering Research Institute, Sheffield Hallam University, United Kingdom

b Zimmer-Biomet UK Limited, Dorcan Industrial Estate, Swindon, United Kingdom

* Corresponding author:
Dr. Arunprabhu Arunachalam Sugumaran
National HIPIMS Technology Centre,
City Campus,
Sheffield Hallam University, Howard Street, Sheffield - S1 1WB, UK.
E-mail: a.arunachalamsugumaran@shu.ac.uk
Telephone: 0114 225 6322

Abstract

Unlike the state-of-the-art plasma nitriding technologies where a low ionisation glow discharge is used, nitriding of CoCrMo alloy was carried out in an industrial size vacuum coater, utilising novel high ionisation, high power impulse magnetron sputtering plasma discharge mixed with unbalanced magnetron sputtering discharge. Three different nitriding voltages were used for the nitriding process. To generate more ions, two pairs of Cr and Nb targets were also operated at low power in $N_{2:}H_2$ gas atmosphere. Dry sliding pin on disc tests were performed at room temperature to measure the coefficient of friction and to estimate the wear coefficient. In the case of samples nitrided at lower nitriding bias voltages such as -700 V and -900 V, the oxidative mild wear mechanism was identified as the dominant wear mechanism. For higher voltage of -1100 V, despite the formation of an oxide based tribolayer severe abrasion was identified as the predominant wear mechanism due to the operation of three body contact wear involving high hardness wear particles. Among the three nitrided samples, the sample nitrided at -900 V was identified as the best with the lowest wear coefficient of Kc = 1.11×10-15 $m^3N^{-1}m^{-1}$ and Knoop microhardness of 2230 $HK_{0.010}$.

Keywords

HIPIMS, Plasma nitriding, Sliding wear behaviour, CoCrMo alloys, mild wear, mixed metal oxides

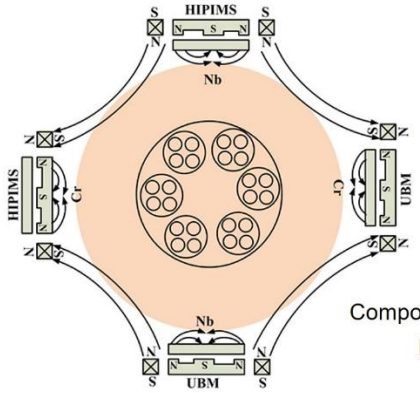

Nitriding by mixed HIPIMS/UBM discharge

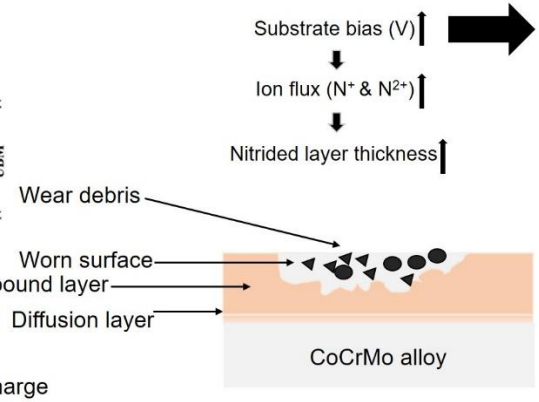

Wear Mechanism – FIB SEM images

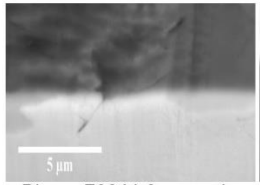

Bias : -700 V, few cracks, mild wear
Kc = 2.18 ×10^{-15} $m^3N^{-1}m^{-1}$

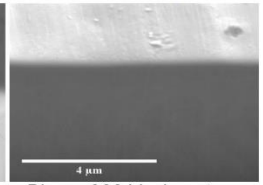

Bias : -900 V, almost no cracks, mild wear
Kc = 1.11 ×10^{-15} $m^3N^{-1}m^{-1}$

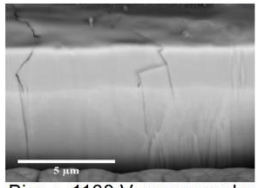

Bias : -1100 V, more cracks, severe wear
Kc = 4.42 ×10^{-15} $m^3N^{-1}m^{-1}$

Raman analysis – wear debris

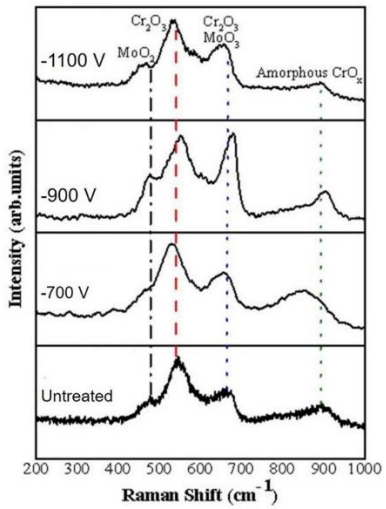

1. Introduction

CoCrMo alloy (ASTM F-75) is widely used for various biomedical applications such as knee implants due to its high fatigue, tensile strength, and superior corrosion resistance. Despite all these advantages, these alloys release toxic, carcinogenic Co and Cr elements during tribo-corrosion, which may induce adverse biological reactions in vivo [1-3]. In addition, the longevity of an implant is dependent on various patient-related factors such as age, certain complicated medical conditions that affect the knee implants and inappropriate day today activities which exert excessive stress on the implants [4]. These factors may lead to revision surgery which is a complex procedure that requires meticulous preoperative planning, specialized implants and tools, and an expert knee surgeon to achieve a good result. According to S. Kurtz et al., by 2030, the number of total knee replacement surgeries is projected to grow by 673% to 3.48 million procedures and the number of knee revisions surgeries is expected to increase by 607% even though the success rate of revision surgeries is very small [5]. Therefore, implant manufacturers are constantly endeavouring to develop a better implant with increased longevity.

In addition to superior corrosion resistance, better tribological properties are vital for eliminating the metal ion release during the tribo-corrosion of the implants in vivo. It is well known that plasma nitriding, a surface hardening technique, produces hard surfaces with enhanced wear resistance and load bearing capacity [6-9]. Ronghua et al. reported the improvement in the wear resistance of CoCrMo alloys by employing a novel high intensity plasma ion nitriding technique, which produced thicker nitrided layers than the conventional plasma nitriding process [6]. Celik et al. reported the near-continuous, well-adhered chromium rich oxide layer formed on the surface enhanced the wear resistance of plasma nitrided CoCrMo alloy [7]. Ba et al. had attributed the adhesive wear mechanism to untreated specimen while assigning the fatigue wear, abrasive wear and slight adhesive wear

mechanisms to nitrided layers [8]. However, publications discussing the mechanisms governing the wear behaviour of plasma nitrided CoCrMo alloy are still very limited. Hence the current research is to shed more light on the evolution of tribolayers and its impact on the wear behaviour of such alloys.

In the current study, a novel low pressure (in the 10^{-3} mbar range, which is three orders of magnitude lower than that of the conventional glow discharge process) mixed high power impulse magnetron sputtering (HIPIMS) and unbalanced magnetron sputtering (UBM) technique was used for the nitriding of CoCrMo alloys. The advantage of using HIPIMS for nitriding is that it can generate highly ionised plasma which facilitates faster nitrogen diffusion. Three different nitriding voltages were used for the nitriding process. Pin on disc dry sliding method has been used to analyse the surface and sub-surface shear behaviour during the wear process and to prediction of the load bearing capacity of the nitrided specimens. This dry sliding wear test is favoured rather than using the simulated body fluid since the best nitrided surface with enhanced properties from this study will undergo a top coating process using mixed HIPIMS/UBM technology, resulting in duplex layers. Hence, the nitrided layer will never encounter the actual synovial fluid in vivo. Nevertheless, it is essential to understand the tribological properties of the nitrided layers to optimize the process parameters for the nitriding process.

2. Experimental details

2.1 Nitriding

HIPIMS enhanced plasma nitriding (HIPN) of CoCrMo (ASTM F75) alloys was carried out in an industrial size physical vapour deposition (PVD) machine (Hauzer Techno Coating 1000-4, The Netherlands) enabled with HIPIMS technology at Sheffield Hallam University. This system is equipped with two HIPIMS power supplies (TRUMPF Hüttinger Elektronic),

two UBM power supplies and a bias power supply with an arc suppression unit [10]. The substrates were subjected to three-fold rotation by mounting on a rotating table located at the centre of the chamber. Prior to the plasma nitriding, surface pre-treatment using HIPIMS plasma discharge was also carried out to remove any kind of native oxide layers from the substrate surface. During this step, the substrates were subjected to intensive bombardment by Ar^+ and Cr^+ ions generated by HIPIMS discharge on a Cr target [11,12]. The nitriding was carried out in a mixed N_2/H_2 (85:15) atmosphere by maintaining HIPIMS discharge on one pair of Cr and Nb targets and UBM discharge on a second pair of Cr and Nb targets for 4 hours. The power applied on both HIPIMS and UBM cathodes was 2 kW. The choice of the target materials was made based on the idea to combine the plasma nitriding step with a coating deposition step in a duplex process carried out in one PVD unit. Our previous research has demonstrated that the nanoscale multilayer CrN/NbN coating deposited on medical implants from non-treated CoCrMo alloy have shown exceptionally high performance, [13] hence the Cr and Nb target material combination. The reactive gas flow rate was precisely controlled using plasma emission monitoring and a control system, "Speedflo" manufactured by Gencoa Ltd. UK. The nitriding voltage was varied from -700 V to -1100 V in order to provide ion bombardment at different energies. The temperature and the total pressure were kept constant at 400 °C and 8.3 x 10^{-3} mbar respectively. Prior to loading into the chamber, samples were mirror polished (1 μm diamond paste) and ultrasonically cleaned in an automated industrial size cleaning line containing several baths with different industrial detergents (alkali solutions) and deionised water to remove all contaminants (mostly organic in nature such as oils) from the surface. The degreased samples were dried in a vacuum chamber at 80 °C for 20 minutes. Three different nitriding voltages of -700 V, -900 V and -1100 V were used for the nitriding process. Hereafter, these samples are called as HIPN-700 V, HIPN-900 V and HIPN-1100 V, respectively.

2.2 Characterization techniques

The following advanced highly precise analytical techniques were employed to characterise the all nitrided and untreated CoCrMo samples.

- A pin on disc tribometer (CSM Instruments SA) was used to measure the dry sliding friction coefficient (μ) at room temperature of about 26 °C and relative humidity of 25%. Various sliding distances such as 0.5 km, 0.75 km, 1 km and 2 km were used to thoroughly understand the evolution of the tribolayer during dry sliding of untreated CoCrMo alloy. This wide range of sliding distances was selected in order to make sure that all the stages of the wear process such as run-in and steady state stage were properly investigated. Tests at shorter sliding distances were also done to avoid perforation of the nitrided layer and thus reading data from a mixed nitrided and substrate material combination was avoided. A 6 mm diameter ball from inert Al_2O_3 material was used as a counterpart under a fixed load of 5 N. The mean value of the three tests was adopted as the result.
- A Dektak-150 stylus profiler (CSM Instruments SA) was used to measure the surface roughness of the samples, profile the wear track and estimate the wear volume loss. Coefficient of wear K_c was calculated using the following relation: K_c = Wear volume loss, (m^3) / Load × Sliding distance, (Nm). This coefficient is based on the assumption that the wear volume varies directly with the contact load and the sliding distance [14].
- A Knoop micro-hardness tester (Mitutoyo) was used to obtain the hardness of the nitrided samples. The applied load was 10 g for all the measurements.
- The thickness of the nitrided layers, surface and subsurface morphology was investigated using a focused ion beam milling enabled scanning electron microscope

(FEI FIB-SEM). Cross-sections and longitudinal sections were prepared by focused ion beam milling using Ga ions at an angle of 52°.

- Energy dispersive spectroscopy was used for the chemical analysis of worn untreated samples.
- X-ray diffraction analysis of worn surfaces of all nitrided and untreated CoCrMo was carried out using an Empyrean X-ray diffractometer (Malvern Panalytical) with Co source. Bragg-Brentano (θ-2θ) geometry was used for the measurements. An optical microscope was used to focus on the area of interest. Special capillary incident beam optics was used to produce a very small sized x-ray beam, thereby increasing the x-ray flux per unit area.
- Raman spectra were recorded using a Horiba Jobin Yvon (HR 800) Raman micro-spectroscope. The sample was irradiated with a green laser of 520 nm wavelength in order to excite the molecules in the region of interest. A 50 % transmission filter was utilized to limit the intensity of the laser. The exposure time of the sample to the laser was approximately 100 S.

3. Results and discussion

3.1 Effect of tribo-layer formation on the tribological properties of untreated CoCrMo alloy

Fig.1 shows the friction curves of untreated CoCrMo alloys obtained from pin on disc dry sliding tests run at various sliding distances. The wear coefficient (K_C) was calculated using the wear volume measured by the Dektak profilometer.

1) 0.5 km sliding distance:

The friction curve for the sample tested at 0.5 km sliding distance, (Fig. 1a) exhibited two different regions: a run-in period followed by the first steady state region. At the start of

the run-in period, the friction coefficient was very low for a short duration due to the presence of an ultra-thin initial air-formed film, which then slowly increased to 0.75 and remained in that range for a while in the first steady state region. This increase in friction coefficient may be attributed to the interaction of the asperity contacts present on the CoCrMo substrate with alumina ball after the removal of the initial air-formed film. Subsequently, the asperity contacts are broken down into fine debris and further fragmented, leading to three body abrasion. The wear coefficient was about 1.1×10^{-13} $m^3N^{-1}m^{-1}$ in this region. The nature of the sliding contact determines the wear regime such as severe and mild. The severe wear observed during the run-in period and first steady state period was due to the direct alumina-CoCrMo metallic contact made in the absence of an oxide film.

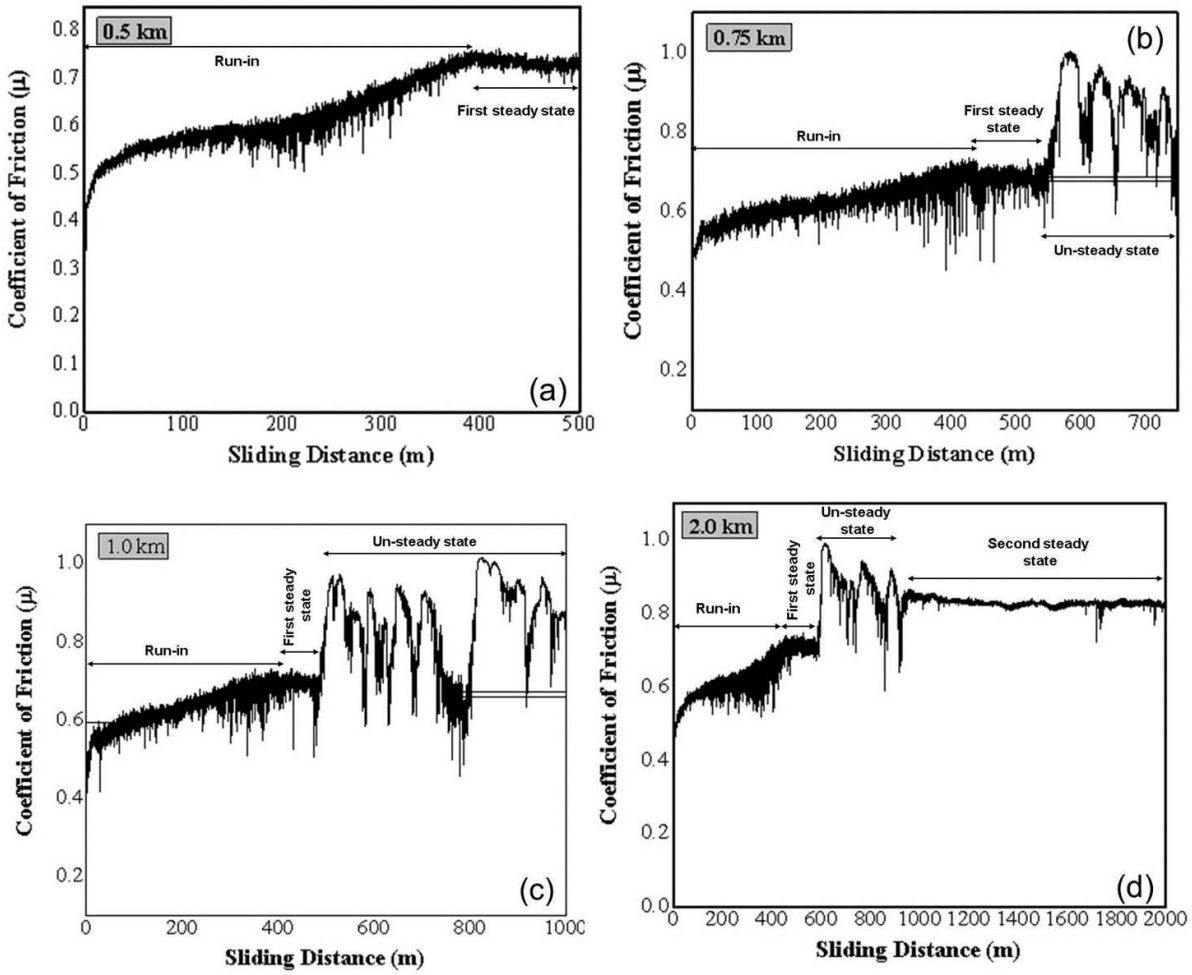

Figure 1. Friction curves of untreated CoCrMo alloy with various sliding distances a) 0.5 km, b) 0.75 km, c) 1 km, d) 2 km

The plan-view SEM micrograph of this sample, Fig. 2a, shows the wide and deep grooves formed due to ploughing, parallel to the sliding direction during abrasive wear (white arrow in the figure indicates the sliding direction). Also, these grooves are found to be filled with pulverized asperity contact wear debris due to their smearing by the stationary counterpart. Generally, the oxidized area looks brighter during SEM observation due to electric charge accumulation as a result of reduced electric conductivity of such a surface. In this sample, the worn area looked little brighter as compared to the unworn area. However, the energy dispersive X-ray (EDX) analysis revealed only the presence of the main alloy elements Co, Cr and Mo but did not detect any oxide formation in the wear track at this stage.

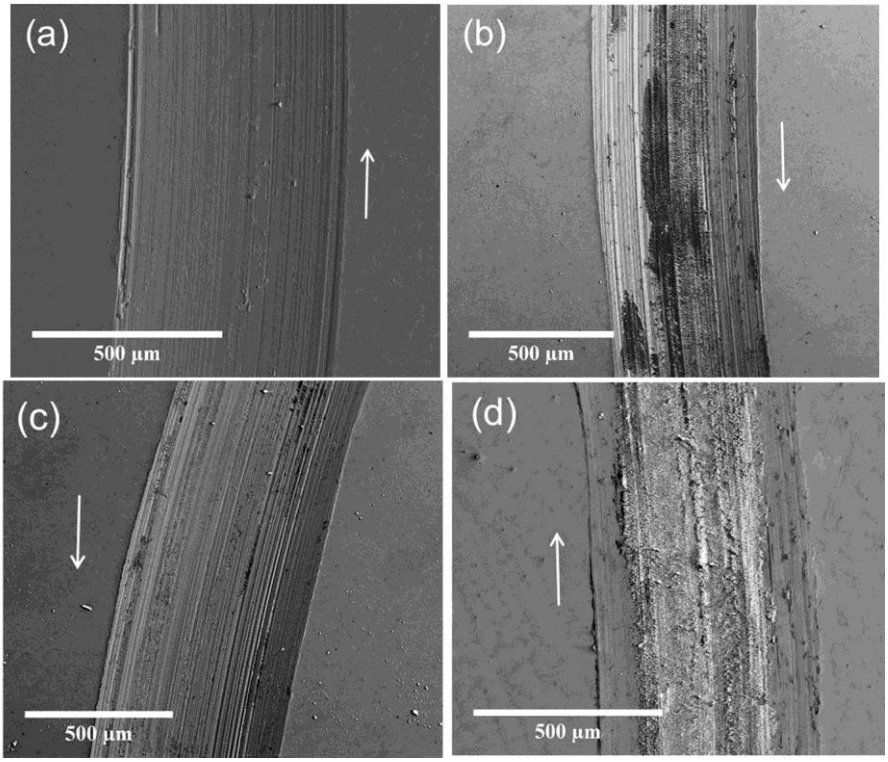

Figure 2. Plan view SEM images of worn surfaces of untreated CoCrMo alloy a) 0.5 km, b) 0.75 km, c) 1 km, d) 2 km

2) 0.75 km and 1 km sliding distance

The friction curve at the longer sliding distance of 0.75 km showed three distinct regions namely run-in, with continuously increasing friction coefficient; steady state where the coefficient of friction remained almost constant followed by an unsteady state region where huge variations of the friction coefficient were observed. The length of the unsteady state region further increased for the sliding distance of 1 km. It is important to highlight that the maximum value of μ in this region was found to be around 1. Generally, the wear debris generated during the run-in period are further compacted into very fine agglomerates while increasing the sliding distance. The volume of the wear debris also increases but more importantly they also intensively oxidize due to the high flash temperatures at the asperity contacts. At the same time, a thin oxide film also grows on the clean worn CoCrMo surface, which is periodically removed, and a fresh clean surface is exposed on each wear traversal. This oxide layer, along with the above said wear debris particles, is then fragmented and compacted onto the worn surface to form slightly raised 'islands'. The area, number and thickness of these islands increase with increasing sliding distance. The complex and repeated interactions between the wear debris, oxide layer and oxide islands with the alumina ball could be the reasons for the unsteady state region with huge fluctuation in friction values. In this region, a transition from a severe to a mild wear regime was observed depending on the extent of the oxide layer formation. The wear coefficient of 0.75 km test was found to be 9×10^{-14} $m^3N^{-1}m^{-1}$ when the worn surface is dominated by non-continuous 'raised islands'. The Kc further decreased to 6.4×10^{-14} $m^3N^{-1}m^{-1}$ when the continuity and compactness of these islands further increased while increasing the sliding distance to 1 km.

Plan-view SEM image (Fig. 2b) of the wear track of 0.75 km sample confirmed that the wear surface was only partially covered with compacted wear debris forming isolated “islands” whereas the remaining surface showed morphology of fine grinding which is

typical for three-body sliding contact wear. Also, Fig. 2c confirmed the formation of a compacted, non-continuous layer when increasing the sliding distance from 0.75 km to 1 km. The worn surfaces appeared to be relatively rough with distinct dark and bright areas (most likely due to the formation of oxides). The observation of oxygen along with the substrate constituents by EDX analysis confirmed that these worn surfaces were in fact oxidized. Cross-section SEM analysis (Fig. 3a and 3b) revealed that the thickness of the islands (0.75 km) and the compacted layer (1 km) was 0.3 µm and 0.7 µm, respectively.

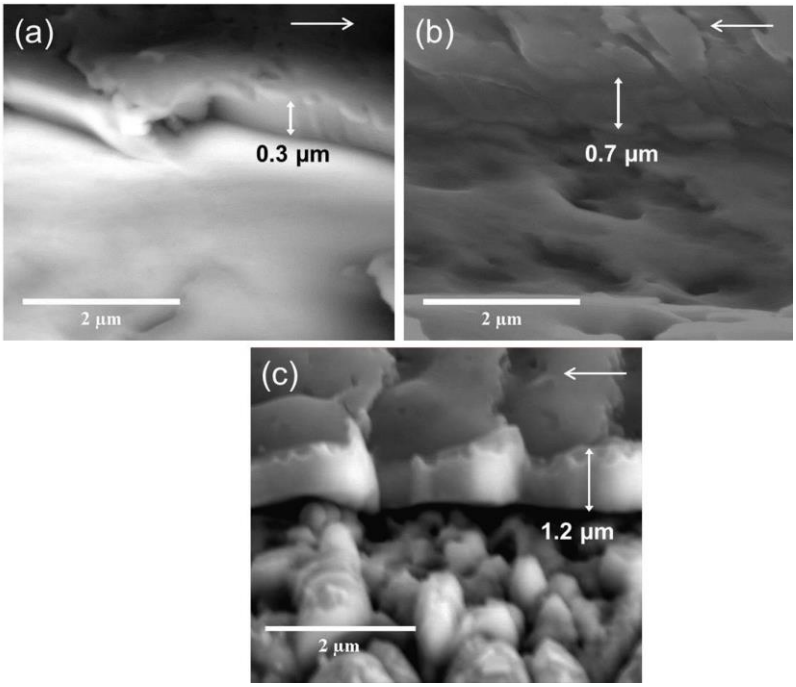

Figure 3. Cross-section SEM images showing tribolayers on the worn surfaces of untreated CoCrMo alloy a) 0.75 km, b) 1 km, c) 2 km

3) 2 km sliding distance

In the second steady state region Fig. 1d, the friction coefficient value dropped considerably to 0.85 immediately after 1 km and continued to slowly drop further with very little variation while increasing the sliding distance to 2 km. The mean µ value was found to be 0.83 and this drop could be attributed to a smooth, near-continuous oxide layer formed as the extent of this layer is further increased in this region. Hence, the CoCrMo substrate made

occasional contact with the alumina counterpart, resulting in a very low Kc value of 2×10^{-14} $m^3N^{-1}m^{-1}$.

The worn surface was found to be much brighter as compared to its counterparts, clearly demonstrating that the surface is heavily oxidized (Fig. 2d). This oxide layer appears to be uniform, compact and near-complete without any interruptions. The EDX analysis also confirmed that this layer is a mixture of oxygen and other substrate elements. The thickness of this layer was about 1.2 μm (Fig. 3c).

In summary, the friction coefficient value increased sharply after 0.5 km and remained high for a while, which then considerably decreased as the sliding progressed. The friction behaviour and the coefficient of friction values in the above explained individual regions remained almost unchanged for all the four sliding distances. All the four curves showed an almost identical run-in period of about 400 m length followed by the first steady state region of about 100 m length. Usually, the friction coefficient tends to be lower in the mild wear regime than that observed in the severe wear regime. However, it has been reported that the oxide layers do not always reduce the friction coefficient [15]. In this study, the friction coefficient in the mild wear regime is found to be higher than that in severe wear. Nevertheless, the growth of the oxide layer decelerated the wear of untreated CoCrMo alloy. The characteristic dry sliding wear mechanisms involving adhesion, abrasion, severe plastic deformation along with oxide tribolayer formation determined the wear behaviour of the CoCrMo alloy at the various stages of sliding test.

3.2 Properties of nitrided and untreated CoCr alloys

3.2.1 Raman and XRD analysis of worn samples

X-ray diffraction and Raman analysis were used to investigate the phase composition of the wear debris formed on the worn surfaces of the untreated CoCrMo substrate and nitrided samples after sliding for 2 km. The Raman spectra of the worn surfaces are shown in Fig 4a. All the samples showed Raman peaks originating from chromium and molybdenum based oxide compounds, however, with slight shift in their positions. Table 1 lists the assignment of various Raman peaks to such oxide compounds. Raman peaks originating from MoO_2 was observed in the 455 cm^{-1} – 480 cm^{-1} region. The characteristic Raman peak of Cr_2O_3 was observed in the range of 532 cm^{-1} to 551 cm^{-1} [16-19]. The peak observed between 650 cm^{-1} and 680 cm^{-1} could be originating from Cr_2O_3 and/or MoO_3 [20-21]. Also, a peak observed between 800 cm^{-1} and 900 cm^{-1} was assigned to various chromium based oxides such as CrO_2, CrO_3 and Cr_8O_{21} as they overlap each other [22-25].

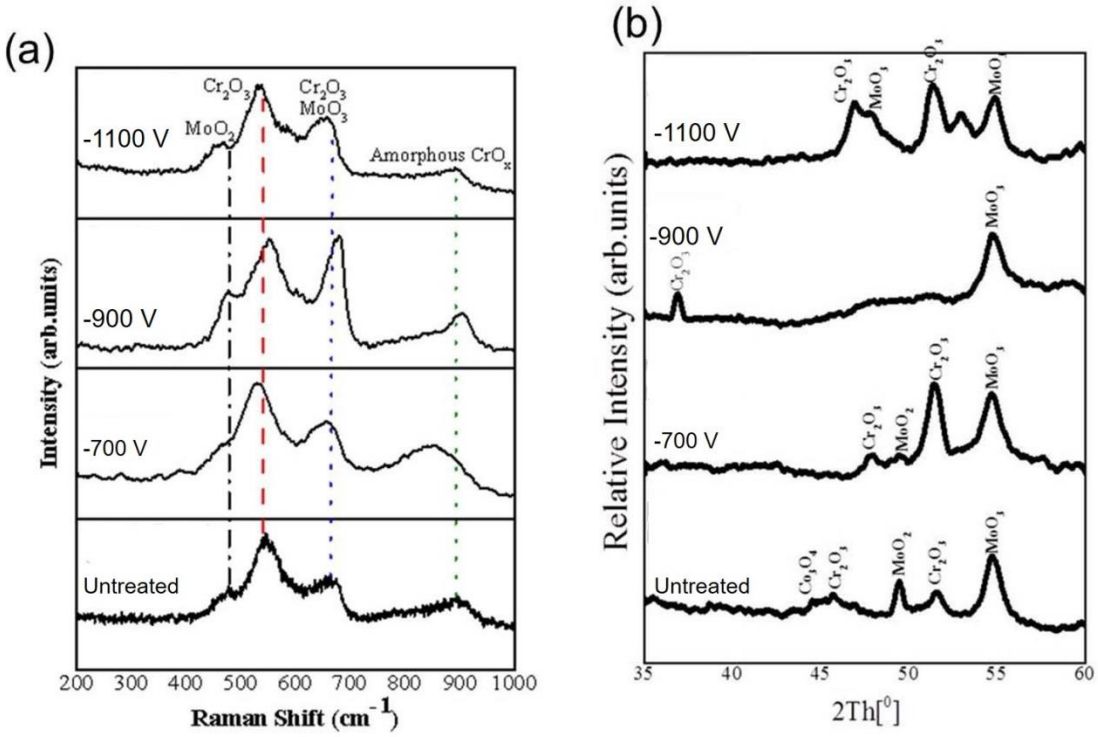

Figure 4. a) Raman spectra and b) XRD diffraction pattern of worn surfaces of various nitrided alloys

Table 1. Assignment of various Raman peaks to respective oxide compounds formed on the worn surfaces of untreated and nitrided alloys (sliding distance: 2 km)

Sample	Raman shift (cm^{-1})	Peak assignment
Untreated CoCrMo substrate	457	MoO_2
	532	Cr_2O_3
	652	Cr_2O_3 and/or MoO_3
	between 800 cm^{-1} and 900 cm^{-1}	Cr based oxides
HIPN-700V	475	MoO_2
	544	Cr_2O_3
	679	Cr_2O_3 and/or MoO_3
	between 800 cm^{-1} and 900 cm^{-1}	Cr based oxides
HIPN-900V	463	MoO_2
	534	Cr_2O_3
	657	Cr_2O_3 and/or MoO_3
	between 800 cm^{-1} and 900 cm^{-1}	Cr based oxides
HIPN-1100V	475	MoO_2
	551	Cr_2O_3
	667	Cr_2O_3 and/or MoO_3
	between 800 cm^{-1} and 900 cm^{-1}	Cr based oxides

Fig. 4 b shows the XRD patterns of worn surfaces after sliding for 2 km. Table 2 shows peak positions and their assignment to respective oxides. Diffraction peaks due to the formation of Cr and Mo based oxide compounds were observed for all the samples including untreated CoCrMo substrate. However, the diffraction patterns of nitrided samples showed significant differences between them in the peak number, peak position and the composition of oxide compounds formed on the worn surfaces. These differences could be mainly due to the degree of oxidation and the nature of the oxide compounds formed on the selected area of interest for the XRD measurement as only a fraction of the worn surface was analysed. The XRD pattern of the untreated CoCrMo substrate also revealed the formation of a Co (major substrate constituent) based oxide compound. These results, along with Raman analysis confirmed that the tribolayers formed on the worn surfaces are indeed oxidized compounds of CoCrMo alloy [26-29]. Also, it is important to that note that both Raman and XRD analyses

did not detect alumina on the worn surfaces of the nitrided specimens. Hence it can be argued that the wear of inert alumina counterpart is marginal.

Table 2 Assignment of various XRD peaks to respective oxide compounds formed on the worn surfaces of untreated and nitrided alloys (sliding distance: 2 km)

Sample	Peak Position	Peak assignment
Untreated CoCrMo substrate	44.2°	Co_3O_4
	45.7°	Cr_2O_3
	48.3°	MoO_3
	52.7°	Cr_2O_3
	54.7°	MoO_3
HIPN-700V	47.4°	Cr_2O_3
	48.6°	MoO_3
	49.9°	MoO_3
	52.7°	Cr_2O_3
HIPN-900V	36.2°	Cr_2O_3
	55.2°	MoO3
HIPN-1100V	45.9°	Cr_2O_3
	46.7°	MoO3
	52.5°	Cr_2O_3
	55.2°	MoO3

3.2.2 Surface morphology of the worn surfaces

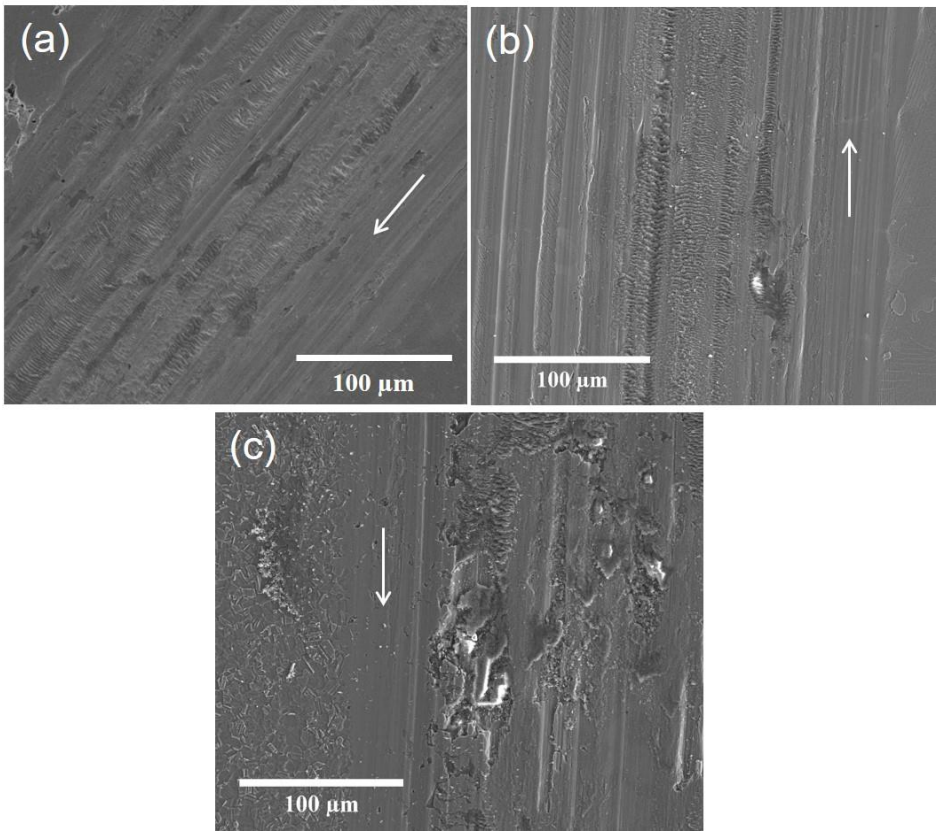

Figure 5. Plan view SEM images showing worn surfaces of CoCrMo alloy (sliding distance: 0.5 km) nitrided at various bias voltages a) -700 V, b) -900 V, c) -1100 V

The dry sliding pin on disc tests of nitrided samples were run for 0.5 km and 2 km to elucidate the effect of sliding distance on the tribological behaviour of the treated alloys. The wear scars generated during these tests were analysed using scanning electron microscopy. The plan view SEM images of the wear tracks of all nitrided samples after sliding for 0.5 km are shown in Figure 5. As explained in Sec. 1, during the initial stages of the tribo-test, the asperities on the surface are ground out and the wear debris oxidized under favourable conditions after the removal of the initial air-formed film. Subsequently, a tribolayer is formed due to the adherence of wear particles to the parent worn surface through the process explained in Section 1. When imaged using SEM, the surface also exhibited dark and bright areas (electric charge due to oxygen). The wear scars of the samples treated with -700 V and - 900 V showed a relatively smooth surface, characterised with shallow grooves and very fine micro cracks, which is typical for fine polishing. This wear behaviour could be due to the

initial smooth surface morphology of these samples with roughness (Ra) values of about 71 nm and 65 nm when nitrided at bias voltages of -700 V and - 900 V respectively. In this case, it can be argued that due to the small size of the wear debris, they do not inflict severe damage by micro-cutting but are mostly compacted onto the worn surface of the parent material in the tribo-contact to form very thin layers. Therefore, it is believed that the predominant wear mechanism in this case is two-body rather than three-body even though the wear debris are still generated. In contrast, the deformation grooves found in the wear tracks on the sample nitrided at higher bias voltage of -1100 V were wider and deeper when compared to HIPN-700 V and HIPN-900 V samples. This difference is attributed to the higher initial surface roughness obtained when higher nitriding bias voltages are applied. The increased roughness in these conditions results from the more intensive bombardment of the nitrided surface by highly energetic N/H and metal ions which produce a significant surface sputtering effect. The roughness is further influenced by the lattice volume expansion due to the incorporation of nitrogen into the metallic lattice during the nitriding process. Therefore, further increase of the surface roughness to Ra = 124 nm due to the application of higher nitriding bias voltage of -1100 V, resulted in severe wear damage due to the operation of three body contact abrasive wear mechanism, Fig 5c. The wear scar in this case was very rough with debris of different shapes as reported by Li et al. [30].

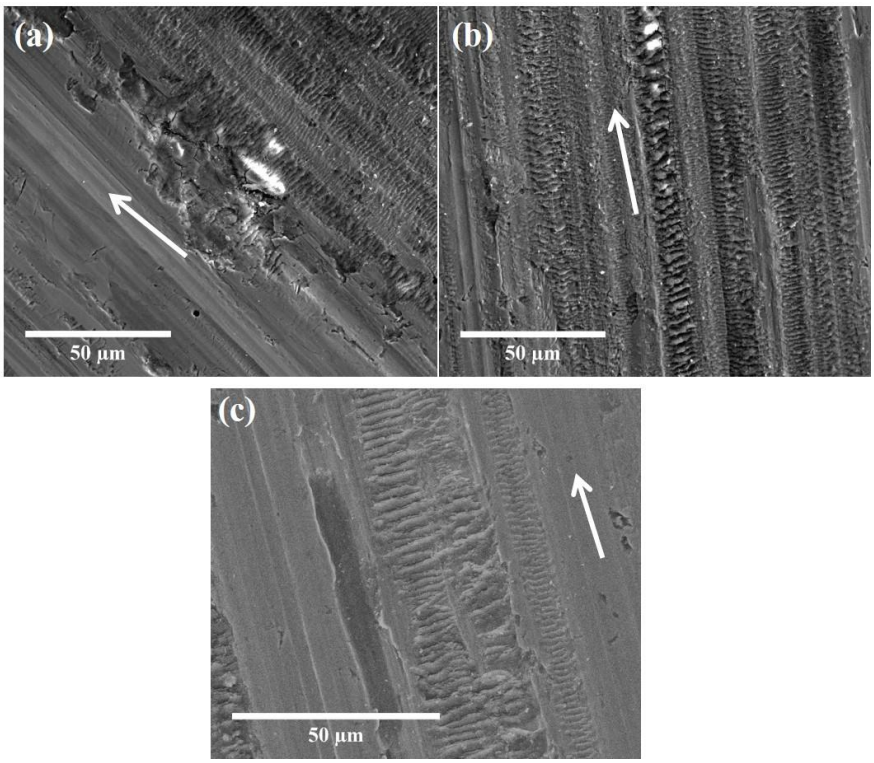

Figure 6. Plan view SEM images showing worn surfaces of CoCrMo alloy (sliding distance: 2 km) nitrided at various bias voltages a) -700 V, b) -900 V, c) -1100 V

Figure 6 summarises the SEM images of the worn surfaces of all nitrided samples after sliding for 2 km. As expected, the extent of the wear damage and oxidation has increased with increasing sliding distance for all three samples.

3.2.3 Subsurface analysis of worn surfaces

The subsurface structure of all nitrided samples after sliding for 2 km was investigated using a Focused Ion Beam milling (FIB) enabled Scanning Electron Microscope. The distinct tribolayers formed on the worn surface of all nitrided samples can be clearly seen in Figure 7. The tribolayer formed on HIPN-700 V sample is comprised of semi-compacted, coarse, small scale wear debris particles generated during dry sliding [Fig. 7a]. On the contrary, the tribolayer formed on HIPN-900 V sample appears to be fully compacted, relatively smooth without any coarse wear debris particles [Fig. 7b]. The HIPN-1100 V sample showed a

tribolayer with an extremely rough surface which consisted of largescale wear debris particles [Fig. 7c].

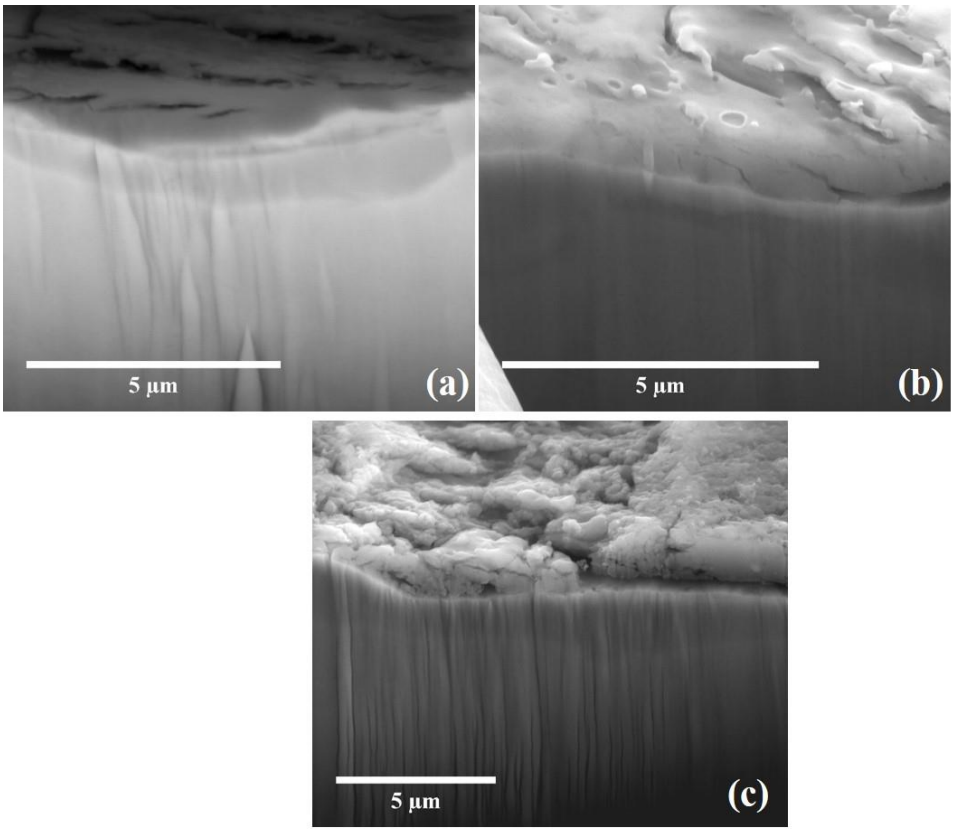

Figure 7. FIB cross-section SEM images showing tribolayers formed on the worn surfaces of CoCrMo alloy (sliding distance: 2 km) nitrided at various bias voltages a) -700 V, b) -900 V, c) -1100 V

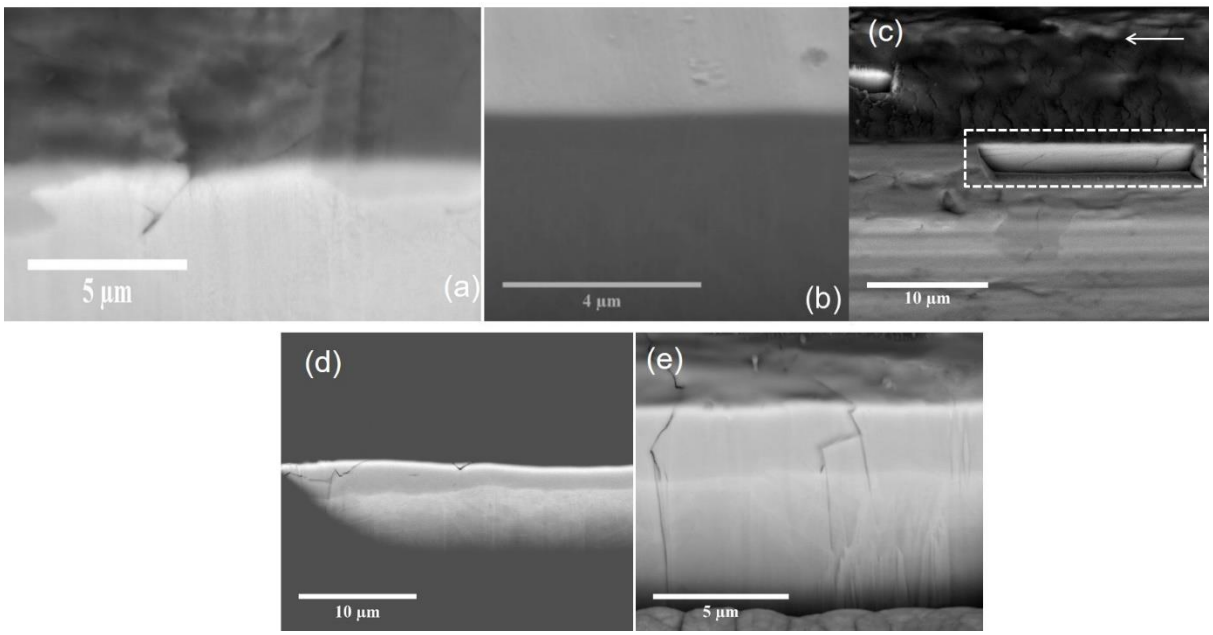

Figure 8. FIB cross-section SEM images showing surface and subsurface morphology of worn areas of CoCrMo alloy (sliding distance : 2 km) nitrided at various bias voltages a) -700 V, b) -900 V, c) -900 V (longitudinal), d) -1100 V, e) -1100 V (longitudinal)

Fig. 8a shows a micro crack initiated on the worn surface of the sample (where the tribolayer appears to be thin) nitrided at -700 V and its propagation towards the soft CoCr substrate. A micro void can also be seen close to the nitrided case-substrate interface. In contrast, no surface initiated or subsurface micro cracks were found in this particular worn area for the HIPN-900 V sample [Fig. 8b]. A thorough investigation of the entire wear track by longitudinal FIB cross sectioning discovered only a few subsurface cracks parallel to the sliding direction, formed due to the shear deformation of the nitrided layer [Fig. 8c]. In comparison with the nitriding at bias voltage of -700 V, the nitriding at higher bias voltage of -900 V has produced a layer with clearly enhanced ductility. However, the nitrided layer ductility deteriorated when the nitriding voltage was further increased. FIB cross sections of the wear track produced in both directions (longitudinal and perpendicular) to the sliding showed that the sample produced at nitriding voltage of -1100 V was severely damaged with

micrographs showing an increased number of surface cracks [Fig. 8d] and cracks propagating through the entire nitride layer towards the substrate [Fig. 8e].

3.2.4 Wear mechanism

Table 3 lists the thickness, microhardness, average coefficient of friction (μ) and coefficient of wear values (Kc) of all samples for both sliding distances. A Knoop micro-hardness tester was used to obtain the hardness of the nitrided samples. The applied load was 10 g for all the measurements. Cross-section SEM analysis were carried out to measure the thickness of the nitrided layers (micrographs not shown here). More information on microhardness and thickness measurements of the nitrided samples can be found in our previous research study [31]. Figure 9 shows the friction coefficient curves of CoCrMo alloy nitride at various bias voltages after sliding for 0.5 km and 2 km respectively. As expected, the μ and Kc values decreased while increasing the sliding distance from 0.5 km to 2 km. However, these values from 2 km tests were considered for the discussion since the effect of the oxide tribo layer is more pronounced at such a long sliding distance. The wear behaviour of nitrided metallic alloys depends on the type (compound and/or diffusion), hardness and thickness of the nitrided layers along with the characteristics of the tribo layer. It is expected that a hard and thick nitrided layer along with a well-adhered smooth top oxide layer would exhibit better wear performance during sliding. In the case of nitrided stainless steel alloys, it has been reported that the diffusion zone is solely responsible for the wear resistance, fatigue strength and the load bearing capacity of steel components in the absence of a compound layer [32].

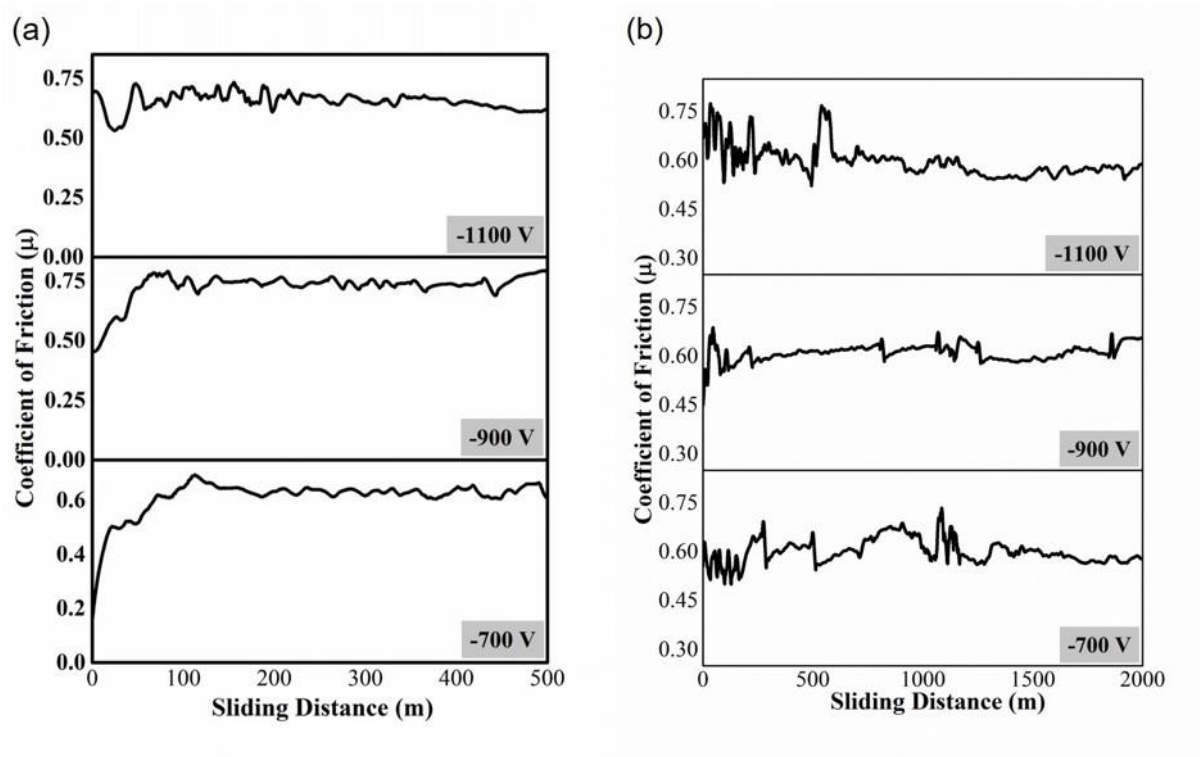

Fig. 9 Friction curves of various nitrided alloys a) 0.5 km b) 2 km

Table 3 Thickness, mechanical and tribological properties of various nitrided alloys

Sample	Thickness µm	Microhardness $HK_{0.010}$	Friction Coefficient (µ)		Wear Coefficient (Kc) $m^3N^{-1}m^{-1}$	
			0.5 km	2 km	0.5 km	2 km
HIPN-700V	1	1400	0.72	0.61	4.2×10^{-15}	2.18×10^{-15}
HIPN-900V	1.8	2230	0.65	0.62	1.98×10^{-15}	1.11×10^{-15}
HIPN-1100V	3.7	2750	0.65	0.59	8.58×10^{-15}	4.42×10^{-15}

As anticipated, all nitrided samples showed increased wear resistance due to increased hardness as compared to untreated CoCrMo alloy. In all the cases, the wear debris generated from the nitrided case participated in the wear process rather than that of inert alumina counterpart as it did not undergo severe wear [Refer Sec. 3.2.1]. The micro crack observed at the nitrided layer/CoCrMo substrate interface in HIPN-700 V sample, (Fig.7a) could be attributed to the fatigue failure at the interface due to tensile stresses developed in the

CoCrMo base material during the sliding test since this is the thinnest nitride layer among the three samples of about 1 µm, including a very thin diffusion layer. The micro hardness of this sample was also found to be very low, in the range of 1400 $HK_{0.010}$. This sample exhibited the µ and Kc values of 0.61 and 2.18×10^{-15} $m^3N^{-1}m^{-1}$, respectively. Despite showing few typical surface and/or subsurface cracks, the sample nitrided at -900 V exhibited the lowest Kc of about 1.11×10^{-15} $m^3N^{-1}m^{-1}$ with µ of 0.62. The microhardness, 2230 $HK_{0.010}$, of this sample is much higher than that of HIPN-700 V sample. Thus, the smooth oxide tribolayer formed on the worn surface is well supported by the underlying 1.8 µm thick hard nitrided layer. It is important to reiterate that this sample generated more nanoscale debris during the asperity contact at the beginning of the wear process due to smooth surface morphology rather than large scale wear debris particles which facilitate severe wear. Hence, in this case, it can be argued that the oxidative mild wear appears to be the dominating wear mechanism rather than micro abrasion. Also, this sample showed a distinct bright, relatively thick diffusion layer beneath the compound layer and clearly enhanced ductility as discussed in 3.2.2. The enhanced ductility of the nitride zone in this case provides for the increased load bearing capacity of such material. Therefore, the synergy of enhanced hardness, oxidative mild wear and ductility resulted in increased load bearing capacity which in turn enhanced the wear behaviour.

It is well understood that using higher nitriding voltages such as -1100 V results in the formation of a thicker nitrided layer with increased hardness which naturally is related to the increased residual stress [33]. The hardness and thickness of this sample was 2750 $HK_{0.010}$ and 3.7 µm, respectively. The increase in the hardness could also be attributed to the formation of Cr_2N compounds (observed by XRD, not shown here) at such high voltages. The formation of Cr_2N compounds at high bias voltages and their effect on the properties of nitrided alloys has been extensively discussed in our previous research work [31]. The

friction and wear coefficient of this sample was 0.59 and 4.42×10^{-15} $m^3N^{-1}m^{-1}$, respectively, which represents a nearly four-fold increase as compared to the HIPN-900 V sample. As already discussed in 3.2.1, this samples produced large scale wear debris particles at the beginning of the wear process as these nitrided layers are very rough, brittle and fragile due to increased hardness and residual stress. These large-scale wear particles further aggravated the wear loss as the sliding progressed. Even though the HIPN-1100 V samples showed almost a factor of two thicker nitrided case compared to HIPN-900 V sample, the wear behaviour was dominated by the combined effect of higher surface roughness, hardness and residual stress levels which lead to poor wear resistance due to the operation of a severe three body micro abrasion wear mechanism rather than oxidative wear despite the formation of oxide tribolayer during sliding.

4. Conclusions

- The wear resistance of the untreated CoCrMo alloy increased while increasing the sliding distance from 0.5 km to 2 km. The coefficient of wear was found to be 2×10^{-14} $m^3N^{-1}m^{-1}$ for 2 km which is one of order magnitude lower than that of 1.1×10^{-13} $m^3N^{-1}m^{-1}$ for 0.5 km. This enhancement could be attributed to the formation of a near-continuous, compact oxide tribolayer for the longest sliding distance of 2 km.
- Raman spectroscopy and XRD analysis of the untreated and nitrided worn surfaces confirmed the formation of substrate material-based oxide components such as Cr_2O_3, MoO_2 and MoO_3. The XRD pattern of the untreated CoCrMo substrate also revealed the formation of Co (major substrate constituent) based oxide compound. The nitrided samples are free of such Co based oxide compounds.
- All the nitrided samples exhibited enhanced wear resistance as compared to the untreated CoCrMo alloy. Among the three nitrided samples, the sample nitrided at -900 V was identified as the best with the lowest wear coefficient of $K_C = 1.11\times10^{-15}$

$m^3N^{-1}m^{-1}$, thickness of 1.8 µm and Knoop microhardness of 2230 $HK_{0.010}$. The wear resistance and the load bearing capacity of the nitrided layers are strongly influenced by its microhardness and ductility. In this case, the oxidative mild wear mechanism was identified as the dominant wear mechanism. The FIB-SEM analysis of the worn area of this sample showed near-scratch free surface and subsurface layers, indicating the enhanced ductility. The synergy of enhanced hardness, oxidative mild wear and ductility resulted in increased load bearing capacity which in turn enhanced the wear behaviour.

- Even though, the HIPN-1100 V sample showed almost a factor of two thicker nitrided case and enhanced hardness value of 2750 $HK_{0.010}$ compared to HIPN-900 V sample, the surface roughness of this sample was very high. In this case, the wear behaviour was dominated by the combined effect of higher surface roughness, hardness and residual stress levels which lead to poor wear resistance due to the operation of a severe three body micro abrasion wear mechanism, involving mainly nitrided layer wear debris rather than oxidative wear despite the formation of oxide tribolayer during sliding.

Acknowledgement

The authors would like to acknowledge Zimmer-Biomet UK for providing financial support for this research. We would also like to thank Mr. Gary Robinson for his technical assistance, Mr. Paul Allender for his assistance in FIB-SEM analysis and Dr. Anthony Bell for his assistance in XRD analysis.

References

1. Y. Okazaki, E. Gotoh, Comparison of metal release from various metallic biomaterials in vitro, Biomaterials. (2005). https://doi.org/10.1016/j.biomaterials.2004.02.005.

2. K.L. Wapner, Implications of metallic corrosion in total knee arthroplasty, Clin. Orthop. Relat. Res. (1991). https://doi.org/10.1097/00003086-199110000-00004.
3. D.B. McGregor, R.A. Baan, C. Partensky, J.M. Rice, J.D. Wilbourn, Evaluation of the carcinogenic risks to humans associated with surgical implants and other foreign bodies - A report of an IARC Monographs Programme Meeting, in: Eur. J. Cancer, 2000. https://doi.org/10.1016/S0959-8049(99)00312-3.
4. O. O'Dwyer Lancaster-Jones, S. Williams, L.M. Jennings, J. Thompson, G.H. Isaac, J. Fisher, M. Al-Hajjar, An in vitro simulation model to assess the severity of edge loading and wear, due to variations in component positioning in hip joint replacements, J. Biomed. Mater. Res. - Part B Appl. Biomater. (2018). https://doi.org/10.1002/jbm.b.33991.
5. S. Kurtz, K. Ong, E. Lau, F. Mowat, M. Halpern, Projections of primary and revision hip and knee arthroplasty in the United States from 2005 to 2030, J. Bone Jt. Surg. - Ser. A. (2007). https://doi.org/10.2106/JBJS.F.00222.
6. R. Wei, T. Booker, C. Rincon, J. Arps, High-intensity plasma ion nitriding of orthopedic materials. Part I. Tribological study, Surf. Coatings Technol. (2004). https://doi.org/10.1016/j.surfcoat.2004.02.052.
7. A. Çelik, Ö. Bayram, A. Alsaran, I. Kayas, A.F. Yetim, Effects of plasma nitriding on mechanical and tribological properties of CoCrMo alloy, Surf. Coatings Technol. (2008). https://doi.org/10.1016/j.surfcoat.2007.08.030.
8. D.C. Ba, L. Xu, Q. Wang, Effects of plasma nitriding ion beam flux density and time on the properties of CoCrMo alloy, Vacuum. (2015). https://doi.org/10.1016/j.vacuum.2015.05.032.
9. H. Dong, S-phase surface engineering of Fe-Cr, Co-Cr and Ni-Cr alloys, Int. Mater. Rev. (2010). https://doi.org/10.1179/095066009X12572530170589.
10. A. Ehiasarian, R. Tietema, R. Bugyi, A. Klimczak, P. Hovsepian, D. Doerwald, A vacuum treatment apparatus, a bias power supply and a method of operating a vacuum treatment apparatus, Patent ZL200780012990.9 in China, granted 10.04.2011, priority date 10.04. 2007., 2007.
11. A.P. Ehiasarian, P.E. Hovsepian, W.D. Munz, Combined coating process comprising magnetic field-assisted, high power, pulsed cathode sputtering and an unbalanced magnetron, US Pat. 7,081,186. 2 (2006). https://www.google.com/patents/US7081186.
12. A.P. Ehiasarian, J.G. Wen, I. Petrov, Interface microstructure engineering by high power impulse magnetron sputtering for the enhancement of adhesion, J. Appl. Phys. (2007). https://doi.org/10.1063/1.2697052.
13. P.E. Hovsepian, A.P. Ehiasarian, Y. Purandare, A.A. Sugumaran, T. Marriott, I. Khan, Development of superlattice CrN/NbN coatings for joint replacements deposited by high power impulse magnetron sputtering, J. Mater. Sci. Mater. Med. 27 (2016) 147. https://doi.org/10.1007/s10856-016-5751-0.
14. D.M. Kennedy, M.S.J. Hashmi, Methods of wear testing for advanced surface coatings and bulk materials, J. Mater. Process. Technol. (1998). https://doi.org/10.1016/s0924-0136(97)00424-x.
15. K. Chen, W. Jiang, X. Cui, S. Wang, Effect of nanoparticles on the tribo-layers and the tribology of a steel-on-steel couple, Proc. Inst. Mech. Eng. Part J J. Eng. Tribol. (2019). https://doi.org/10.1177/1350650118765005.
16. J. Singh, V. Verma, R. Kumar, Preparation and structural, optical studies of Al substituted chromium oxide (Cr2O3) nanoparticles, Vacuum. (2019). https://doi.org/10.1016/j.vacuum.2018.09.033.

17. M. Mohammadtaheri, Q. Yang, Y. Li, J. Corona-Gomez, The effect of deposition parameters on the structure and mechanical properties of chromium oxide coatings deposited by reactive magnetron sputtering, Coatings. (2018). https://doi.org/10.3390/coatings8030111.
18. L. Xin, Y. Lu, T. Shoji, The comparative study on nanostructured tribolayers of Alloy 690TT subjected to fretting wear under different oxygen contents, Mater. Charact. (2017). https://doi.org/10.1016/j.matchar.2017.04.034.
19. M. Roy, S. Ghosh, M.K. Naskar, Solvothermal synthesis of Cr2O3 nanocubes via template-free route, Mater. Chem. Phys. 159 (2015) 101–106. https://doi.org/10.1016/j.matchemphys.2015.03.058.
20. L. Kumari, Y.R. Ma, C.C. Tsai, Y.W. Lin, S.Y. Wu, K.W. Cheng, Y. Liou, X-ray diffraction and Raman scattering studies on large-area array and nanobranched structure of 1D MoO2 nanorods, Nanotechnology. (2007). https://doi.org/10.1088/0957-4484/18/11/115717.
21. S. Patel, K. Dewan an, S. Srivastav, N. Verma, P. Jena, A. Singh, N. Gajbhiye, Synthesis of α-MoO_3 nanofibers for enhanced field-emission properties, Adv. Mater. Lett. 9 (2018). https://doi.org/10.5185/amlett.2018.2022.
22. S. Kikuchi, K. Kawauchi, M. Kurosawa, H. Honjho, T. Yagishita, Non-destructive rapid analysis discriminating between chromium (VI) and chromium (III) oxides in electrical and electronic equipment using Raman spectroscopy, Anal. Sci. (2005). https://doi.org/10.2116/analsci.21.197.
23. O. Monnereau, L. Tortet, C.E.A. Grigorescu, D. Savastru, C.R. Iordanescu, F. Guinneton, R. Notonier, A. Tonetto, T. Zhang, I.N. Mihailescu, D. Stanoi, H.J. Trodahl, Chromium oxides mixtures in PLD films investigated by Raman spectroscopy, J. Optoelectron. Adv. Mater. (2010).
24. M.N. Iliev, A.P. Litvinchuk, H.G. Lee, C.W. Chu, A. Barry, J.M.D. Coey, Raman spectroscopy of ferromagnetic CrO2, Phys. Rev. B - Condens. Matter Mater. Phys. (1999). https://doi.org/10.1103/PhysRevB.60.33.
25. D. Stanoi, G. Socol, C. Grigorescu, F. Guinneton, O. Monnereau, L. Tortet, T. Zhang, I.N. Mihailescu, Chromium oxides thin films prepared and coated in situ with gold by pulsed laser deposition, in: Mater. Sci. Eng. B Solid-State Mater. Adv. Technol., 2005. https://doi.org/10.1016/j.mseb.2004.12.016.
26. P. Hones, M. Diserens, F. Lévy, Characterization of sputter-deposited chromium oxide thin films, in: Surf. Coatings Technol., 1999. https://doi.org/10.1016/S0257-8972(99)00384-9.
27. P. Prieto, J.F. Marco, A. Serrano, M. Manso, J. de la Figuera, Highly oriented (111) CoO and Co_3O_4 thin films grown by ion beam sputtering, J. Alloys Compd. (2019). https://doi.org/10.1016/j.jallcom.2019.151912.
28. D. Wu, R. Shen, R. Yang, W. Ji, M. Jiang, W. Ding, L. Peng, Mixed Molybdenum Oxides with Superior Performances as an Advanced Anode Material for Lithium-Ion Batteries, Sci. Rep. (2017). https://doi.org/10.1038/srep44697.
29. I. Esparza, M. Paredes, R. Martinez, A. Gaona-Couto, G. Sanchez-Loredo, L.M. Flores-Velez, O. Dominguez, Solid State Reactions in Cr2O3-ZnO Nanoparticles Synthesized by Triethanolamine Chemical Precipitation, Mater. Sci. Appl. 02 (2011) 1584–1592. https://doi.org/10.4236/msa.2011.211212.
30. C.X. Li, T. Bell, Sliding wear properties of active screen plasma nitrided 316 austenitic stainless steel, Wear. (2004). https://doi.org/10.1016/j.wear.2003.07.006.
31. K. Shukla, A.A. Sugumaran, I. Khan, A.P. Ehiasarian, P.E. Hovsepian, Low pressure plasma nitrided CoCrMo alloy utilising HIPIMS discharge for biomedical

applications, J. Mech. Behav. Biomed. Mater. (2020). https://doi.org/10.1016/j.jmbbm.2020.104004.
32. E.J. Mittemeijer, Fundamentals of Nitriding and Nitrocarburizing, ASM Handbook, Vol. Steel Heat Treat. Fundam. Process. (2013).
33. P.E. Hovsepian, A.A. Sugumaran, Y. Purandare, D.A.L. Loch, A.P. Ehiasarian, Effect of the degree of high power impulse magnetron sputtering utilisation on the structure and properties of TiN films, Thin Solid Films. (2014). https://doi.org/10.1016/j.tsf.2014.04.002.

Author Statement

Arunprabhu Arunachalam Sugumaran: Experiment and Draft preparation. **Krishnanand Shukla:** Experimental work, data collection, processing and analyses, draft preparation**. Imran Khan:** Defining the research idea**. A. P. Ehiasarian:** Leading the HIPIMS research. **P. Eh Hovsepian:** Technology and material development.